Copy No. _____

Defence Research and Development Canada
Recherche et développement pour la défense Canada

DEFENCE R&D DÉFENSE

Bonded-Patch Integrity Characterization: A Modal Resonance Approach

Gino Rinaldi
NSERC Research Fellow

Marc Genest
NRC-IAR

Defence R&D Canada – Atlantic

Technical Memorandum
DRDC Atlantic TM 2009-079
September 2009

Canada

This page intentionally left blank.

Bonded-Patch Integrity Characterization: A Modal Resonance Approach

Gino Rinaldi
NSERC Research Fellow

Marc Genest
NRC-IAR

Defence R&D Canada – Atlantic

Technical Memorandum
DRDC Atlantic TM 2009-079
September 2009

Principal Author

Original signed by Gino Rinaldi

Gino Rinaldi

NSERC Research Fellow

Approved by

Original signed by Ken McRae

Ken McRae

Head / Air Vehicles Research Section

Approved for release by

Original signed by Ron Kuwahara for

Dr. Calvin V. Hyatt

Chief Scientist / DRDC Atlantic

Abstract

Bonded-patch technology can be employed to either enhance the integrity or to repair damaged structures. In aerospace applications consideration must be given to the effectiveness of the bonded-patch technology to restore the performance of a given component to an acceptable level. Repair of aircraft and components is of particular importance for military air fleets due to the prolonged life-cycle of the aircraft beyond the normal design life. In this respect, a reliable and cost-effective repair technology would help to minimize costs associated with maintenance of military air fleets by offering a low cost alternative to replacing aircraft components. A fundamental drawback to the application of this technology, particularly for critical, primary structure, is the need to assure that the patch is performing as designed. Hence, the on-component characterization of a given bonded-patch is of vital importance in terms of assessing the integrity of the bond. Disbond or delamination associated with long-term stress cycling can adversely affect the quality of the bonded-patch. In this report, a simple and reliable method based on modal resonance is described in which the variation in the modal resonance is employed to detect and monitor the evolution of a bonded-patch disbond. For demonstration purposes the proposed method is applied to aluminum 6061-T651 beams with bonded-patch segments on their surface.

Résumé

La technologie des rapiéçages collés peut servir à améliorer l'intégrité des structures endommagées ou à les réparer. Dans le domaine aérospatial, il faut tenir compte de la capacité de cette technologie à ramener le rendement d'un composant donné à un niveau acceptable. La réparation des aéronefs et des composants revêt une importance particulière pour les flottes aériennes militaires en raison de la prolongation de la durée de vie des aéronefs au-delà de leur durée de vie normale. À cet égard, une technologie de réparation fiable et rentable aiderait à réduire au minimum les coûts liés à la maintenance des flottes aériennes militaires en offrant une solution de rechange peu coûteuse au remplacement des composants d'aéronef. Un des principaux inconvénients liés à l'utilisation d'une telle technologie, plus particulièrement au niveau des structures primaires critiques, est la nécessité de faire en sorte que le rapiéçage fonctionne comme prévu. La caractérisation sur place d'un rapiéçage collé est donc d'une importance vitale du point de vue de l'évaluation de l'intégrité du collage. Le décollement associé au stress cyclique à long terme peut nuire à la qualité du rapiéçage collé. Le présent rapport traite d'une méthode simple et fiable qui se sert des variations de la résonance modale pour déceler et surveiller l'évolution des décollements de rapiéçage. Aux fins de démonstration, la méthode proposée est appliquée sur des poutres en aluminium 6061-T651 comportant des rapiéçages collés en surface.

This page intentionally left blank.

Executive summary

Bonded-Patch Integrity Characterization: A Modal Resonance Approach

Rinaldi, G. and Genest, M.; DRDC Atlantic TM 2009-079; Defence R&D Canada – Atlantic; September 2009.

Introduction or background

Fatigue damage, hidden cracks, disbonded joints, erosion, and corrosion are among the major flaws encountered in today's bridges, buildings, space transport vehicles, and fleet of aging aircraft. Aircraft operate in conditions that can vary significantly (pressure, temperature, vibrations, take-off and landing) over a relatively short period of time. As the quantity of aircraft that continue to operate beyond their design lives increases, the number of flight-cycles continues to increase. This augments the likelihood that flaws develop throughout the aircraft's skin and airframe components due to these intrinsic flight-cycles.

The specific costs associated with the increasing maintenance and repair of aging aircraft are rising at an unexpected rate. In this regard, condition-based maintenance practices can be employed to replace the current time-based maintenance approach. Current viewpoints towards damage-tolerance oblige a structure to be capable of withstanding small damage without failure. Also, new and unexpected structural damage must be addressed by the application of advanced detection methods. Hence, there is a need for reliable structural health monitoring (SHM) systems that can assess the structural condition of the part and, if need be, signal the need for maintenance intervention.

Composite bonded patch repairs continue to be one of the most cost-effective alternatives to the very high replacement costs of aircraft components and to their life extension, but quick, easy and reliable integrity assessment tools have yet been established for that type of repairs. In this work, the proposed SHM approach is based on a simple mechanical vibration induced by tapping the specimen of interest, but employs advanced experimental modal analysis tools to determine patch disbond integrity, severity and progression. By monitoring the vibration produced the damage assessment can determined.

Results

A simple, practical, deployable technique based on modal analysis is demonstrated on simple aluminium 6061-T651 patched beam specimens to characterize composite bonded repairs disbond severity and propagation. It is demonstrated that the frequency shift can be correlated to the percentage of disbond and that at higher frequencies provides better resolution. In addition, two sets of calibration curves were also presented to compensate for frequency shift that could result from other factors.

Significance

The proposed approach presents a real potential for integration into a maintenance program due to its analysis and implementation simplicity as well as system portability. Moreover the proposed approach is quick and inexpensive, which can reduce maintenance cost associated with inspection and maintenance of bonded repairs.

Future plans

The proposed approach was demonstrated on a simple sample which uses Teflon film to simulate patch disbonds. It is planned to demonstrate the same approach to determine patch disbond integrity, severity and progression while a patch repairs is undergoing fatigue cycle. Thereafter, a demonstration on real aircraft structure is expected.

Sommaire

Bonded-Patch Integrity Characterization: A Modal Resonance Approach

Rinaldi, G. and Genest, M.; DRDC Atlantic TM 2009-079; R & D pour la défense Canada – Atlantique; September 2009.

Introduction ou contexte

Les dommages causés par la fatigue, les criques cachées, les joints décollés, l'érosion et la corrosion comptent parmi les principaux problèmes qui affectent les ponts, les bâtiments, les véhicules spatiaux et les flottes d'aéronefs vieillissants. Les conditions dans lesquelles volent les aéronefs peuvent varier rapidement et de manière significative (pression, température, vibrations, opérations de décollage et d'atterrissage). Puisque le nombre d'aéronefs exploités au-delà de leur durée de vie utile augmente, le nombre de cycles de vol augmente aussi, ce qui fait accroître les possibilités de défaillance au niveau des revêtements des aéronefs et des composants des cellules.

Les coûts liés au nombre toujours croissant de travaux de maintenance et de réparation des aéronefs vieillissants grimpent à une vitesse étonnante. Pour contrôler la situation, il est possible d'utiliser des méthodes de maintenance basées sur l'état plutôt que les méthodes en vigueur basées sur la durée. Selon les points de vue actuels sur la tolérance aux dommages, une structure doit pouvoir résister à des dommages mineurs sans qu'il y ait défaillance. De plus, de nouveaux dommages structuraux imprévus exigent l'utilisation de méthodes de détection de pointe. Il faut donc des systèmes de surveillance de l'état des structures fiables capables d'évaluer l'état des pièces et, le cas échéant, de déterminer les besoins de maintenance.

Le rapiéçage des composites collés constitue toujours une des solutions de rechange les plus rentables pour faire face aux coûts de remplacement très élevés des composants d'aéronef en permettant de prolonger la durée de vie des composants. Par contre, il n'existe pas d'outils capables de faire des évaluations rapides, faciles et fiables de l'intégrité en vue d'effectuer ce type de réparation. La méthode de surveillance de l'état des structures proposée dans le présent document est fondée sur une simple vibration mécanique produite en frappant sur un échantillon, mais elle fait appel à des outils d'analyse modale expérimentaux et évolués pour déterminer l'intégrité, la gravité et l'évolution des décollements de rapiéçage. En examinant la vibration produite, il est possible d'évaluer les dommages.

Résultats

Une technique simple, pratique et utilisable sur le terrain, basée sur une analyse modale, a été utilisée sur de simples éprouvettes de poutre rapiécée en aluminium 6061-T651 afin de caractériser la gravité et la propagation des décollements de rapiéçages de composites collés. Il a été démontré qu'il était possible de mettre le déplacement de fréquence en corrélation avec le pourcentage de décollement et que la résolution était meilleure aux fréquences élevées. De plus,

deux ensembles de courbes d'étalonnage ont également été présentés pour compenser le déplacement de fréquence qui pourrait résulter d'autres facteurs.

Importance

L'approche proposée présente un potentiel réel d'intégration dans un programme de maintenance en raison de la simplicité de son analyse et de sa mise en œuvre, de même que de la portabilité du système. De plus, l'approche proposée est rapide et peu coûteuse, et peut permettre de réduire les coûts liés à l'inspection et à la maintenance des rapiéçages collés.

Perspectives

L'approche proposée a été démontrée grâce à une simple éprouvette comportant une pellicule de Téflon qui simule les décollements de rapiéçage. La même approche devrait être utilisée pour déterminer l'intégrité, la gravité et l'évolution des décollements de rapiéçage alors qu'un rapiéçage est soumis à une fatigue cyclique. Par la suite, une démonstration devrait être effectuée sur une véritable structure d'aéronef.

Table of contents

List of figures

List of tables

Acknowledgements

The authors would like to thank Mr. Brian Moyes and Mr. Thomas Benak in the preparation of the aluminum beams and in the setting up of the thermal experiments. The authors would also like to acknowledge Mr. Mike Brothers for his help in the experimental testing.

This page intentionally left blank.

1. Introduction

1.1 Background

Fatigue damage, hidden cracks, disbonded joints, erosion, and corrosion are among the major faults encountered in today's bridges, buildings, space transport vehicles, and fleet of aging aircraft. Aircraft operate in conditions that can vary significantly (pressure, temperature, vibrations, take-off, landing) over a relatively short period of time [1]. The number of flight-cycles continues to increase as aircraft lifetimes are extended beyond their design limits, and the quantity of aircraft, both military and civilian, that continue to operate well beyond their design lives continues to grow.

An inescapable consequence of the extended use of aircraft is that flaws (cracks, corrosion, impact damage) develop throughout the aircraft's skin and airframe components due to these intrinsic flight-cycles. The purchasing of new aircraft or components is often delayed resulting in aging aircraft fleets that in turn place ever increasing demands on efficient and safe repair methods [1]. In addition to the costs associated with normal operational costs, further expenses associated with the increasing maintenance and surveillance needs of aging aircraft are rising at an unexpected rate. Maintenance and repairs account for about a quarter of aging commercial aircraft operating costs. In this regard, condition-based maintenance practices can be employed to replace the current time-based maintenance approach. Such condition-based systems should be able to detect developing, and monitor existing damage before disastrous failures occur [2].

Current viewpoints towards damage-tolerance oblige a structure to be capable of withstanding small damage without failure [2]. Also, new and unexpected structural damage must be addressed by the application of advanced detection methods. Hence, there is a need for reliable structural health monitoring systems that can assess the structural condition of the part and, if need be, signal the need for maintenance intervention.

1.2 Structural health monitoring

The basic concept is to build a monitoring scheme similar in concept to the human nervous system, with a network of sensors placed in critical areas where structural integrity must be maintained [3]. In this way structural health monitoring (SHM) comprises a distributed network of sensors capable of collecting and sending information. SHM sensor systems work by detecting the presence of damage using an onboard sensor network, or by recording or tabulating the incidence, if any, of high risk events such as impact. The main point to note is that the relative ease of monitoring an entire network of distributed sensors means that structural health assessment can occur more often, thereby allowing operators to be even more informed with respect to the onset of damage [2]. A number of SHM sensing technologies are currently under development or in use. The most common among them are the following [3]:

i) Fibre Bragg Diffraction Grating Sensors: Fibre-optic cables embedded in the structure are marked with optical interference patterns. Any local strain causes a slight change in the sensor's transmitted light wavelength.

ii) Acoustic Emission: Transducers listen for acoustic signals generated by cracks, delaminations or fibre breakage.

iii) Acousto-Ultrasonics: Low Frequency acoustic pulses are sent through a part and received by transducers. Damage causes a change in the reflected acoustic energy.

iv) Smart or Sensitive Coatings: Coatings or paints with integrated piezo- and ferro-electric elements or carbon nanotubes can function to detect strain. Some sort of spectroscopy is needed to detect changes in the coating.

v) Microwave Sensors: Small microwave sensors embedded in the structure send and receive signals that indicate moisture ingress. The method is good for monitoring composite sandwich structures.

vi) Imaging Ultrasonics: A small ultrasonic wave transducer generates a signal that passes through the material. Changes in wave reflection indicate flaws or damage.

vii) Comparative Vacuum Monitoring: Monitoring of vacuum vs. atmospheric pressure in fine tubes within a simple manifold that is adhered to the surface of a structure can detect crack propagation in that structure.

The concept of the distributed sensor network for aircraft is shown in Figure 1.

Figure 1: A depiction of a distributed sensor network for structural health monitoring on a CF-18 fighter aircraft. CF aircraft figures taken from [4].

1.3 Bonded patch repair

Traditionally, aircraft repairs have been accomplished by mechanically fastening or adhesively bonding metallic or composite doublers to the problem area. The use of bonded composite materials offers the airframe manufacturers and aircraft maintenance facilities a cost effective method to safely extend the lives of their aircraft or component. However, although adhesive bonding repair presents several advantages over mechanical fastening, including reduced stress concentration, greater structural efficiency and improved aerodynamic profiles, it is not possible to assure the initial quality and on-going integrity of the repair. Over the past two decades, adhesive bonding repair technology has advanced significantly and new concepts such as smart patch repairs technology have been introduced to address such technology limitations [1-3, 5,6].

The "smart" concept is based on the integration of advanced sensors within the repair. For this purpose, several sensors have been investigated, including piezoelectric film sensors, optical-fibre sensors and traditional resistive strain gauges [7-10]. Even though these sensors have presented a real potential for the development of such smart-concept, they also introduced additional manufacturing and implementation complexity, potentially needing additional certification requirements. Due to these challenges, several efforts have recently focused on the development and evaluation of new sensing approaches. Such approaches include integrated strain gauge strips that are used for accumulated damage and cycle exposure of the adhesively bonded repair [11], wireless strain gauge adhesive bonded repair delamination and disbond [12], piezoelectric based bonded repair structural health monitoring [13-15] among others. Although these new and innovative approaches introduce additional benefits, they are mainly being developed for on-line structural health monitoring and they require further development for the application considered in this work.

1.3.1 Disbond detection methods

As discussed above, several nondestructive inspection (NDI) methods are available for damage assessment and integrity evaluation of composite structures; however, traditional inspection methods often require that the structure be taken out service in order for the evaluation to be carried out. In this regard, continuous SHM allows assessment of the health of the structure without removing the structure from service [16]. In recognizing the fact that composite bonded patch repairs continue to be one of the most cost-effective alternatives to the very high replacement costs of aircraft components and to their life extension, and that quick, easy and reliable integrity assessment tools are needed, a conventional NDI is introduced and assessed.

In this work, the proposed SHM approach is based on the well known "tap-test" [17, 19-21] but it employs advanced experimental modal analysis tools [18] to determine patch disbond integrity, severity and progression. A tap is applied manually to the structure of interest (for the work presented herein, aluminum 6061-T651 beams with bonded carbon fibre composite patches are employed as test structures). Then by monitoring if there is a variation in the vibrational resonance of the structure, a determination can be made as to whether there is any damage present in the structure. The proposed approach presents a real potential for integration into a maintenance program due to its analysis and implementation simplicity as well as system portability.

1.4 Carbon fibre composites

The quantity of fibre-composite materials being used in aerospace, industrial, automotive and marine structures is increasing every year. Their primary attributes are that they offer higher stiffness and strength compared with conventional engineering materials [22]. Shown in Figure 2 is a schematic of the fabrication process for carbon fibre composite materials [23].

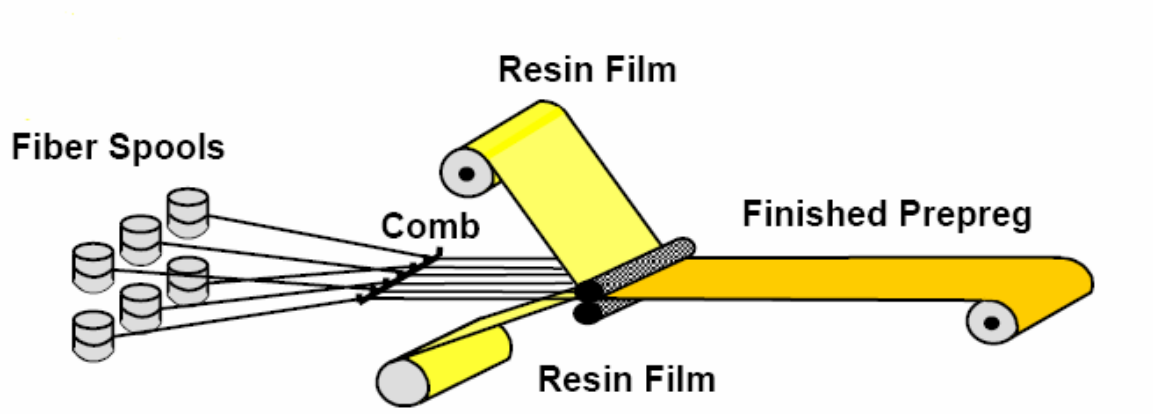

Figure 2: An overview of the manufacturing process for carbon fibre composites [23].

1.4.1 AS4/3501-6

The bonded patch material employed in this work is the graphite/epoxy AS4/3501-6 composite. In this alpha-numeric designation the AS4 refers to the carbon or graphite fibres, and the 3501-6 to the type of epoxy used. The finished product is then known as the AS4/3501-6 composite. Shown in Figure 3 is the coordinate system used to designate the orientation of the fibres within the composite [24]. In this figure, the principle axis are designated numerically as *1*-along the length of the fibre; *2*-parallel to the laminate; *3*-perpendicular to the laminate. The rotational axes are designated as X, Y, and Z are used to characterize any fibre misalignments from the principle axes. In this regard, the mechanical properties for AS4/3501-6 composites are depended upon the orientation and alignment of the carbon/graphite fibres within the composite. Typical mechanical constants are shown in Table 1, where $E_1$and E_2 are Young's modulus in the *1* and *2* directions, respectively, G_{12} the shear modulus in the *1-2* plane, and ν_{12} Poisson's ratio in the *1-2* plane.

Table 1: A comparison of mechanical constants for AS4/3501-6 carbon fibre composite.

Mechanical Constants	[25]	[26]	[27]	[28]
E_1 *(GPa)*	138	142	131	142
E_2 *(GPa)*	9.65	10.3	13	10.3
G_{12} *(GPa)*	5.24	7.2	6.4	7.2
ν_{12}	0.3	0.27	0.34	0.27
Density (kg/m^3)	1550	1580	-	1580

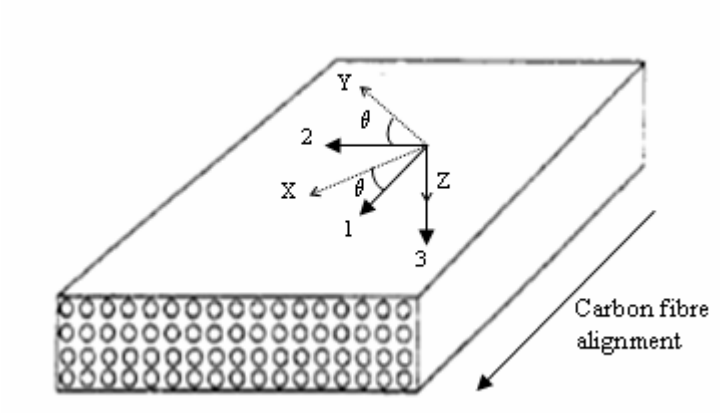

Figure 3: Schematic of a carbon fibre composite illustrating the principal axes that define the fibre orientation and alignment [24].

The effects of fibre misalignment on the mechanical constants are shown in Figure 4 [29].

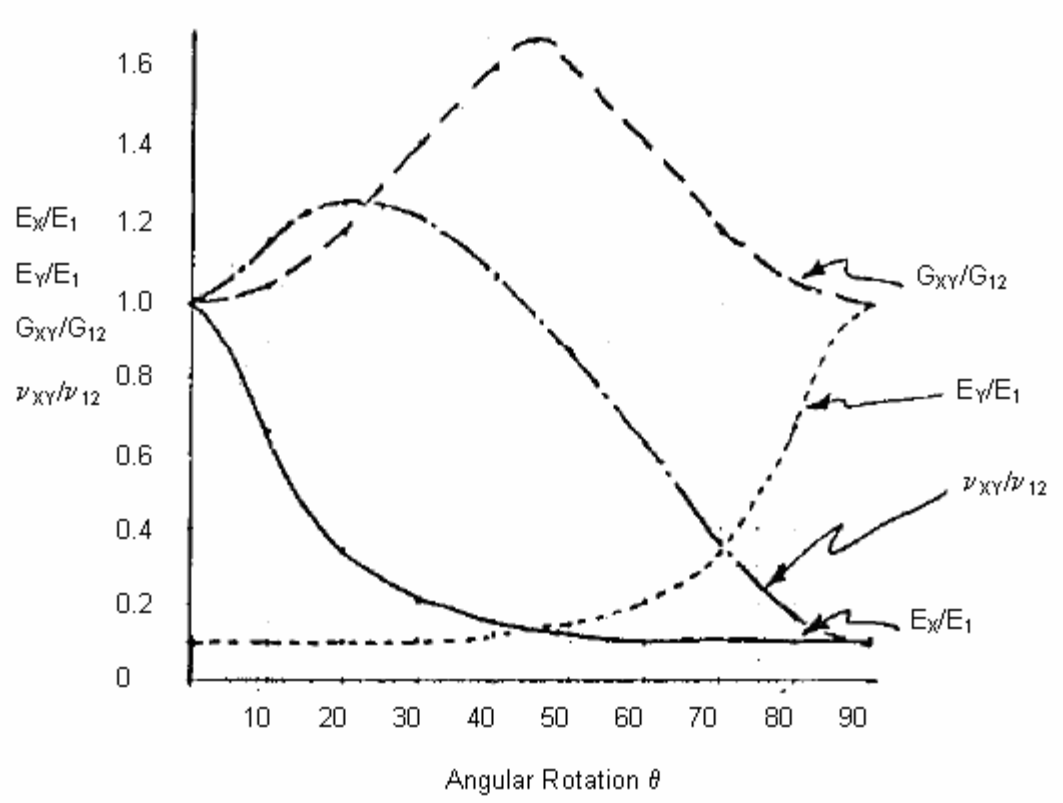

Figure 4: The effect of carbon fibre misalignment on the mechanical constants of the composite [29].

1.4.2 Comparing chemical structures: carbon, graphite

AS4 fibres can have either carbon or graphite designations. At first glance this would appear to be the same material as graphite is basically carbon. However, subtle differences between these two forms of carbon do exist and they are discussed below.

Carbon fibres are amorphous hence, it is difficult to get an accurate description of the atomic structure. A very small piece of carbon fibre has a "chickenwire" like configuration of its atoms and can look like graphite, as shown in Figure 5 [30]. The main difference, however, is that carbon fibres do not have long range ordering of the chickenwire structure as does graphite as illustrated in Figure 6 [31].

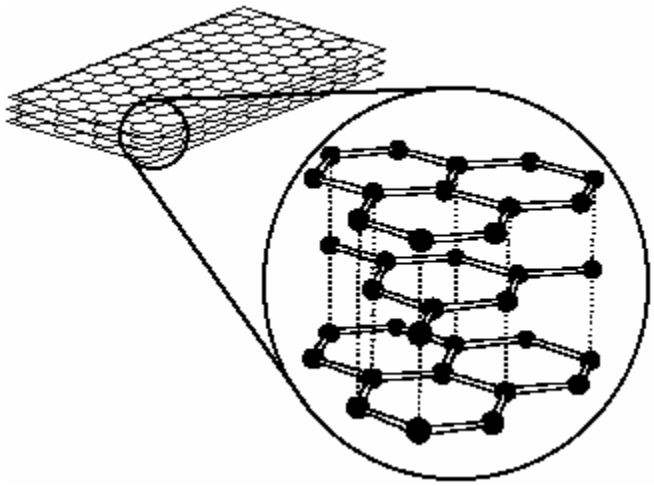

Figure 5: Chickenwire like atomic arrangement in carbon fibres [30].

It has been reported that the inclusion of graphite nano-particles in the carbon fibre/epoxy composite can improve the mechanical properties of the composite [31].

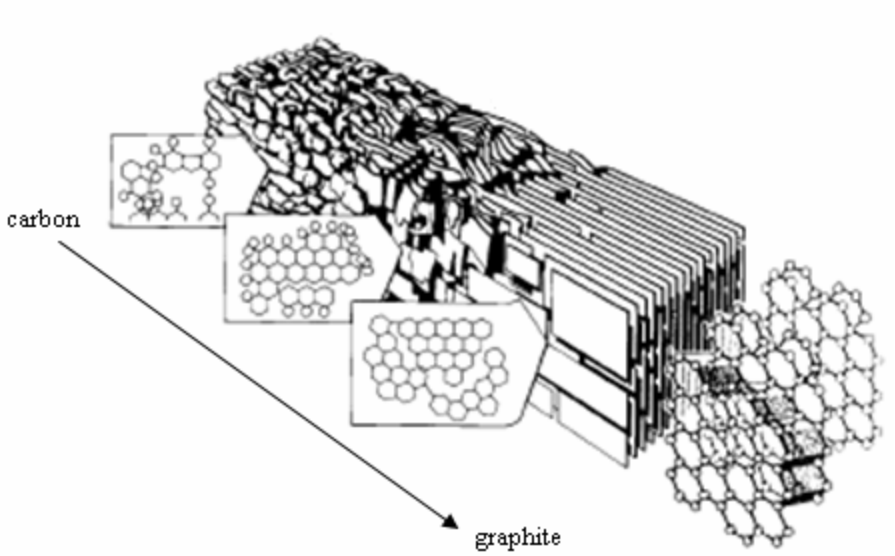

Figure 6: Comparing the structure of amorphous carbon fibres to the highly organized graphite fibres [30].

2. Beam Patching Methodology

To demonstrate the suitability of the proposed approach for the detection of composites bonded patch repair disbond severity and progression, an experimental analysis is conducted on several patched aluminum (Al) specimens. In these particular beams the patches are used primarily to add rigidity.

2.1 Bond patched Al 6061-T651 beams

The specimens consist of Al 6061-T651 substrates having dimensions (length x width x thickness) of 406.4 x 50.8 x 6.35 mm^3 with 6-ply AS4 3501-6 graphite/epoxy (Gr/Ep) adhesively bonded repair patches tapered at 0.059 (rise/run). Figure 7, illustrates a schematic of the designed and manufactured bonded repair specimens as well as an unpatched specimen that is used as a reference. The patches are centered symmetrically about the mid-point of each beam. Teflon inserts, only on one side of the repair, are used to simulate bondline disbond. Five specimen configurations were considered: unpatched (Figure 7f), no-disbond (Figure 7e), quarter-disbond (Figure 7d), half (Figure 7c) and full (Figure 7b) disbonds and are designated as B00, B01, B03, B05 and B07, respectively.

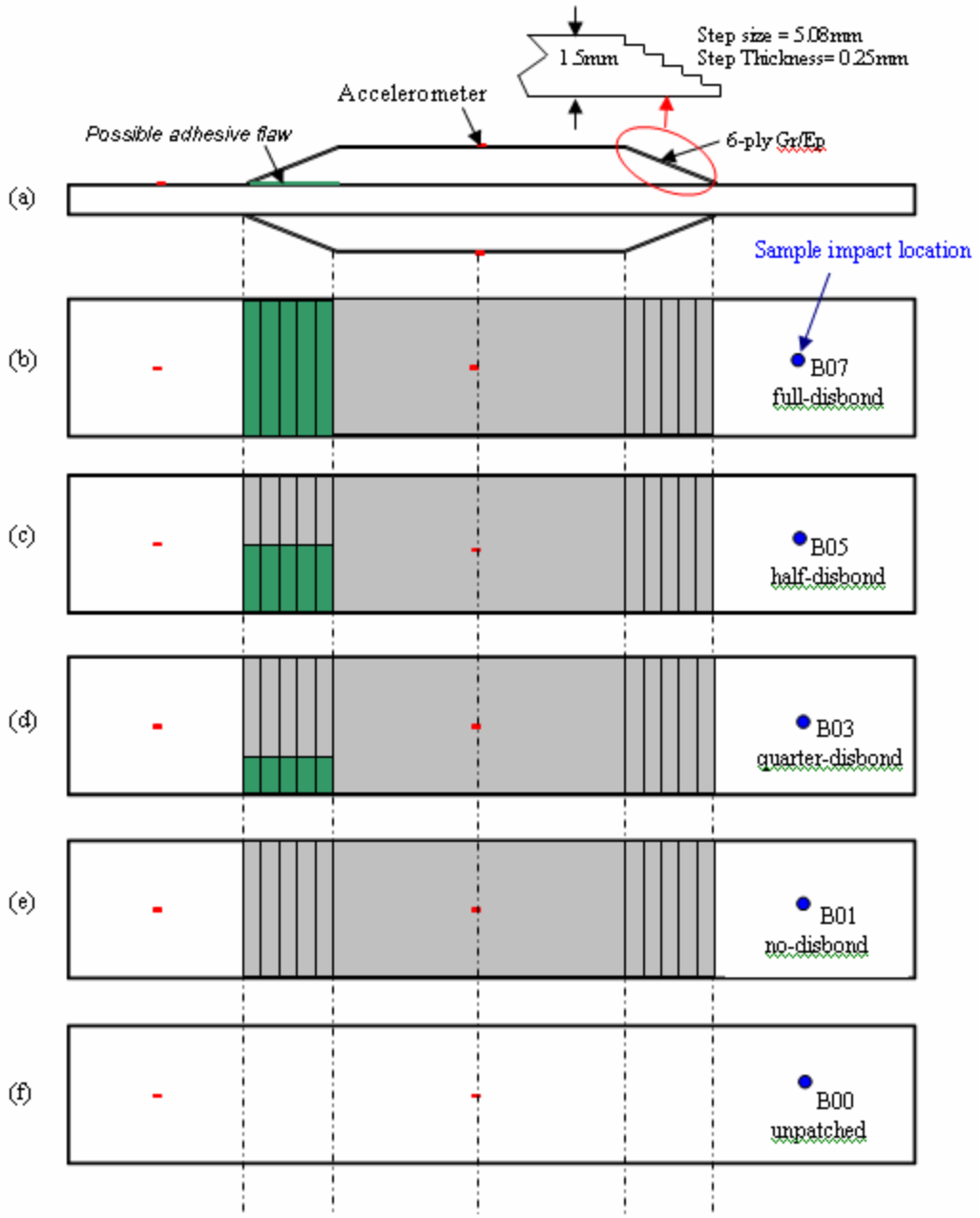

Figure 7: The various investigated patched specimens configurations. (a) Side view of the beam with bonded patch and orientation of Teflon disbond insert. (b) Top view of full width disbond. (c) Top view of ½ width disbond. (d) Top view of ¼ width disbond. (e) Top view of no disbond. (f) Top view of unpatched bare aluminum beam.

The patches are bonded onto the specimen in a symmetric configuration to ensure no specimen bending due to thermal effect experienced during the manufacturing process. Furthermore, the patches used in this study are purely for strength enhancement rather than damage repair. The

101.6 x 50.8 mm^2 AS4/3501-6 Gr/Ep patches were manufactured using the carbon fibre manufacturer (Hexcel) recommended process cycle and following the common lay-up and de-bulking processes for composites laminates manufacturing (Ramp P/T 116°C dwell 65 min @ 85 psig, 177°C dwell 130 min @ 100 psig with heat up rate of +1.9°C/min and cool down rate of 1.9°C/min). Cytec FM®73 film adhesive [32] of thickness 0.18 mm is used to bond these patches (both sides) to the Al substrate. To create a disbond between the patches and the substrate, a rectangular cut-out in the FM®73 adhesive layer, corresponding to the desired disbond configuration is made. A patch of 0.05 mm thick, non-perforated Teflon film is placed in the adhesive cut-out area between the carbon fibre patch and the Al substrate to ensure successful disbond. Excess of the Teflon film is left extending from the patch perimeter to facilitate removal following cure. Thereafter, the vacuum bagged patched Al substrates are cured in an autoclave environment. This entailed ramping pressure up to 5 psig, venting the vacuum bag, then commence the temperature and pressure ramp to 121°C @ 40 psig, 121°C dwell of 65 min 121°C @ 40 psig with heat up rate of +2.4 to 2.8°C/min and cool down rate of 2.4 to 2.8°C/min, all under a vented state. Figure 8 illustrates the manufactured specimens highlighting the disbonded regions. Shown in Figure 9 is an overview of the experimental setup employed for the disbond characterization.

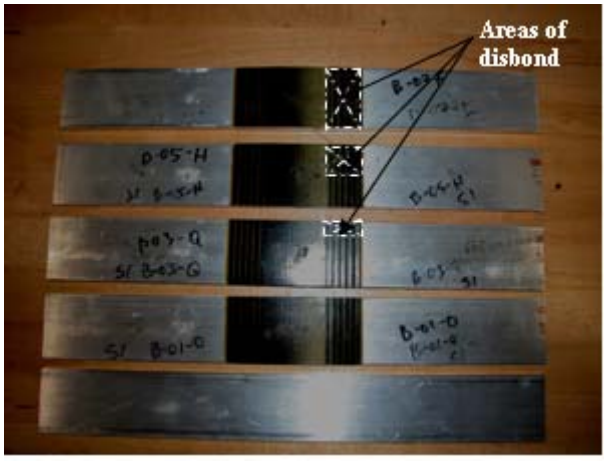

Figure 8: The five Al 6061-T651 tested specimens.

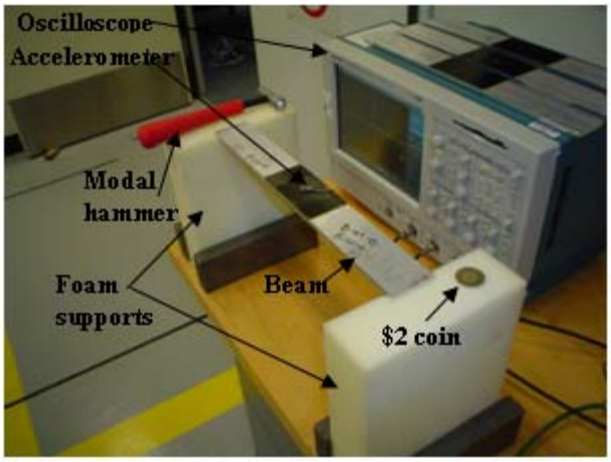

Figure 9: Experimental setup for the modal approach.

3. Experimental Setup and Analysis

It is well known that when patching the substrates the structure's stiffness increases. Additionally, any induced damage to the patch (patch disbond or delamination) causes reduction in its stiffness. It is the objective of this experimental analysis to employ the proposed frequency based modal approach and to monitor the frequency response to infer and monitor the disbond and its progression.

3.1 Base excitation

Employing the experimental setup of Figure 9, the proposed modal based approach is demonstrated. For this experiment, a set of three accelerometers (Brüel & Kjær Type 4517) with amplifiers (Wilcoxon Research Model P703B) were placed as shown in Figure 7 and used to detect the repair response to different degrees of disbond. A modal analysis impact hammer (Endevco Model 2302-100) with it associated signal amplifier (Endevco Model 4416B) was employed to inject base excitation energy into the system. An oscilloscope (Tektronix Model TDS 5104) is used to acquire and analyze the impact as well as the accelerometers time domain response signals. The time domain signals are then converted to a frequency response through a Fast Fourier Transform (FFT) algorithm within the TDS 5104. Shown in Figure 10 is a schematic of the B00 beam and foam support structures employed for simulating free-free boundary support conditions.

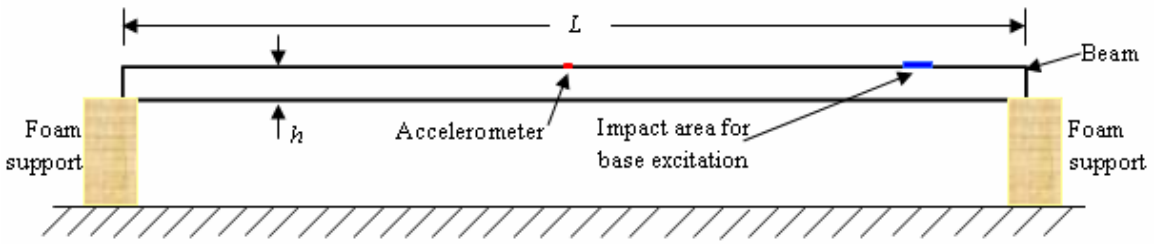

Figure 10: A schematic of the unpatched aluminum B00 beam indicating the placement of the accelerometer and base excitation impact location.

The manufactured specimens (beams) of Figures 7 and 8 were individually impacted, at the specified locations, using a modal hammer and the frequency responses were obtained using accelerometers. The beam ends were supported by soft foam braces (shown in Figure 9) to simulate free-free boundary support conditions. The first experimentation consisted of impacting the reference beam (B00), as shown in Figure 10, with individual high and low energy impacts. This was done to illustrate the effect of impact energy on the frequency response. Figure 11 shows examples of high (top) and low (bottom) energy impacts and their respective frequency responses and illustrates only changes of amplitude for all frequencies at these impact levels. In this figure, the left hand side of both the top and bottom shows the impact hammer response.

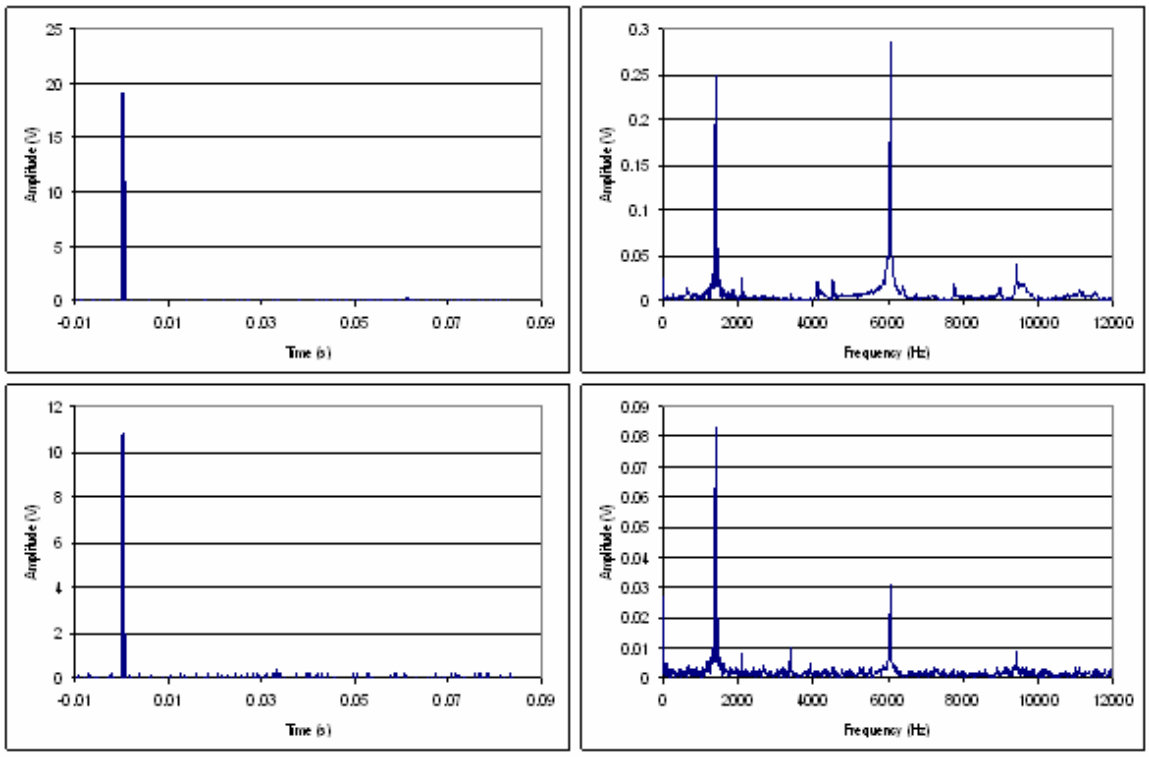

Figure 11: The effects of modal impact hammer energy on the frequency response. Top row: High energy impact. Bottom: Low energy impact.

In order to demonstrate the simplicity of this modal approach for disbond characterization, a "coin tap" test is proposed in order to excite the specimen's natural frequencies. Figure 12 shows a comparison of impact hammer and coin tap tests (a $2 coin was employed).

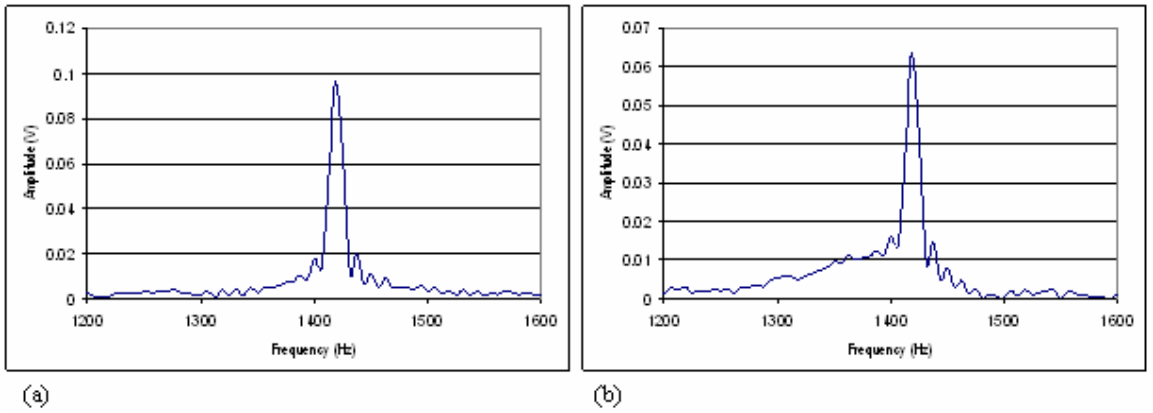

Figure 12: A comparison of the frequency response obtained using (a) an impact hammer and (b) a coin tap.

Comparing the two base excitation approaches, it can be seen that they are virtually identical in terms of the natural frequency response obtained. The only difference is seen in the amplitude of the signal obtained due to the relatively "heavier" impact obtained with the hammer.

3.1.1 Accelerometer placement

Presented here is the effect of the placement of the accelerometer on the frequency response obtained. In this regard, three accelerometer positions, as shown in Figure 13, and designated as *Beam*, *Top*, and *Bottom*, respectively are investigated. The impact location for the base excitation is also shown in this figure. The B03 beam was employed in this investigation. The frequency responses obtained from these individual accelerometers are shown in Figure 14. In this comparison, there is no discernable difference in the frequency response other than in the amplitude of the signals obtained from each individual accelerometer. This may in part be due to slight variations in each accelerometer's sensitivity, and also to the damping effects of the bonded patch material.

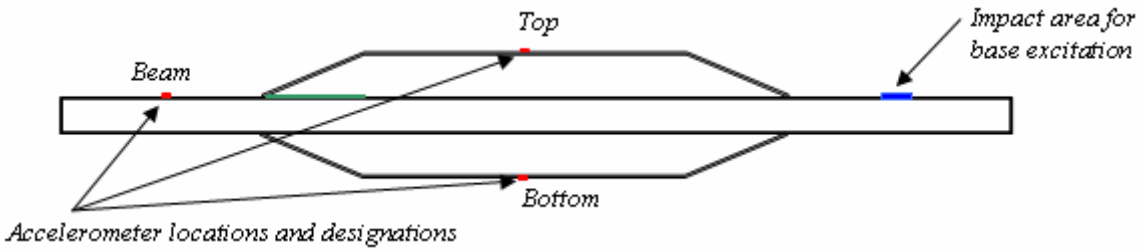

Figure 13: A schematic of the patched aluminum beam indicating the placement of the accelerometers and base excitation impact location.

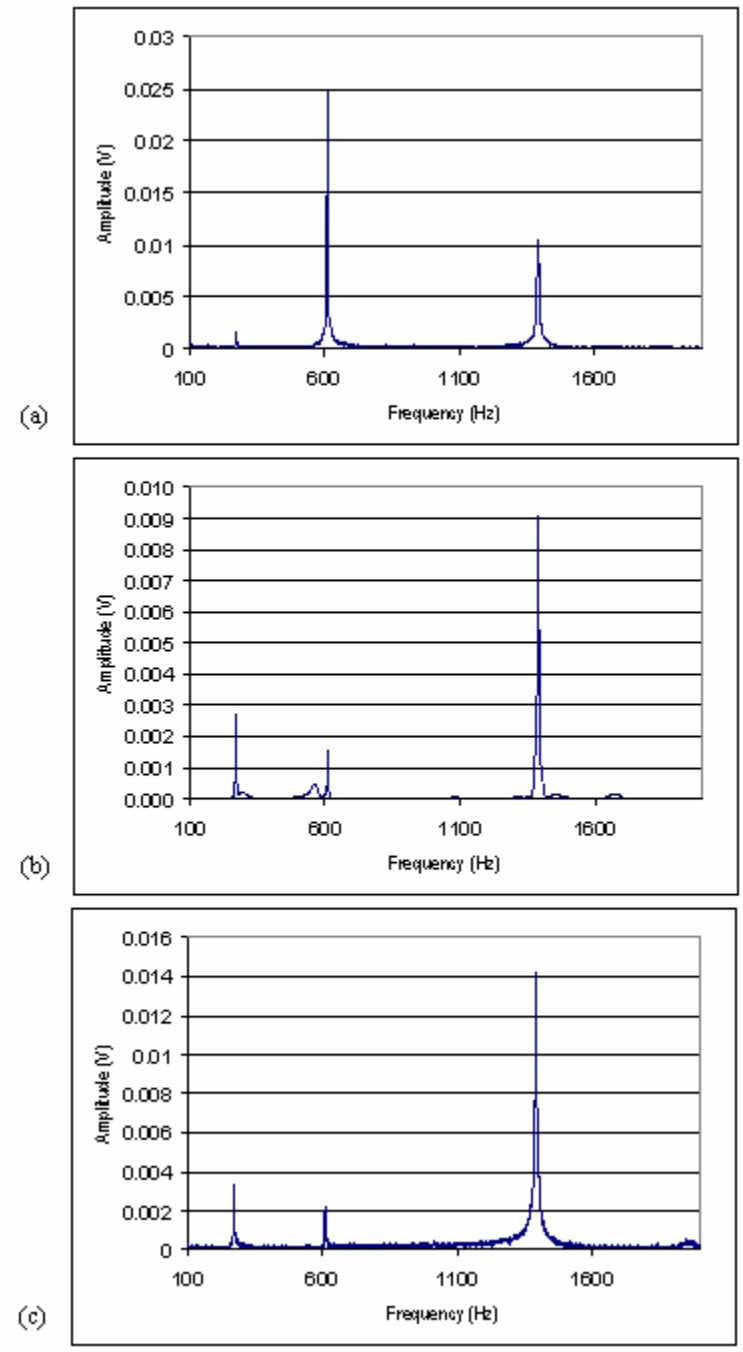

Figure 14: A comparison of the frequency responses obtained for the three accelerometer placements. (a) Beam. (b) Top. (c) Bottom.

3.1.2 Impact location

The effect of the location of the base excitation impact is now investigated. This is done to show that depending upon the location of the individual impacts; certain frequencies may be amplified or, contrarily, attenuated. In this regard, five impact positions *a*, *b*, *c*, *d* and *e* as shown in Figure 15 are compared. Hence, in order to apply this modal approach, it will be necessary to establish an "ideal" impact location for the duration of the tests. The results obtained for the B01 beam are presented in Figure 15.

These results illustrate the influence of the impact location on the excited frequencies. Hence, if one is to monitor the patch disbond employing a change in the 3414 Hz frequency (for this particular accelerometer-impact location configuration) then one may impact the beam at location *a*, *b*, *d* and *e*. At location *c*, the 3414 Hz frequency is completely non-responsive with respect to the location of the accelerometer. In this regard, once one has made a choice of impact location for any given specimen, then one should maintain that particular location in order to be able to quantify any changes to the beam specimen. Similar effects are seen for the other frequencies with amplitudes increasing/decreasing as a function of the modal hammer impact location.

3.2 Structural enhancement

While the main focus of bonded patch repair technology is to repair a structure, a secondary but equally important application is to add structural enhancement to a given component (damaged or not). In terms of the modal response analysis approach presented herein, the increased structural strength may be quantified through an increase in the stiffness of the structure which may in turn be characterized by an increase in the natural frequency obtained for that structure. An example of this phenomenon is shown in Figure 16 for the unpatched B00 and the patched no disbond B01 beams.

3.3 Disbond characterization

With all the necessary tools and knowledge acquired from the previous tests conducted, it is now the aim to apply the modal approach to detect and quantify the amount of disbond present. For these tests the same experimental setup as shown in Figures 9-10 was adopted. The accelerometer placement chosen was the *Top* location as shown in Figure 13 and base excitation impact location *b* as shown in Figure 15 was used. Frequency bands of 200-290 Hz (band *1*), 1140-1440 Hz (band *2*), and 2850-3450 Hz (band *3*) were targeted to monitor the shift in frequency due to disbond progression. Also, the increased stiffness due to the bonded patch can be seen in each frequency band. Illustrated in Figure 17 are the frequency responses for all the cases considered in Figure 7. In all frequency ranges it is observed that, by bond patching the Al beams, the beams' stiffness increased and the frequencies have shifted significantly. For the frequency shown in Figure 17c, a shift of 15.2% is observed between the unpatched specimen (B00) and the no disbond specimen (B01). Hence, the stipulated increase in stiffness due to patching can be clearly quantified using the frequency based modal response.

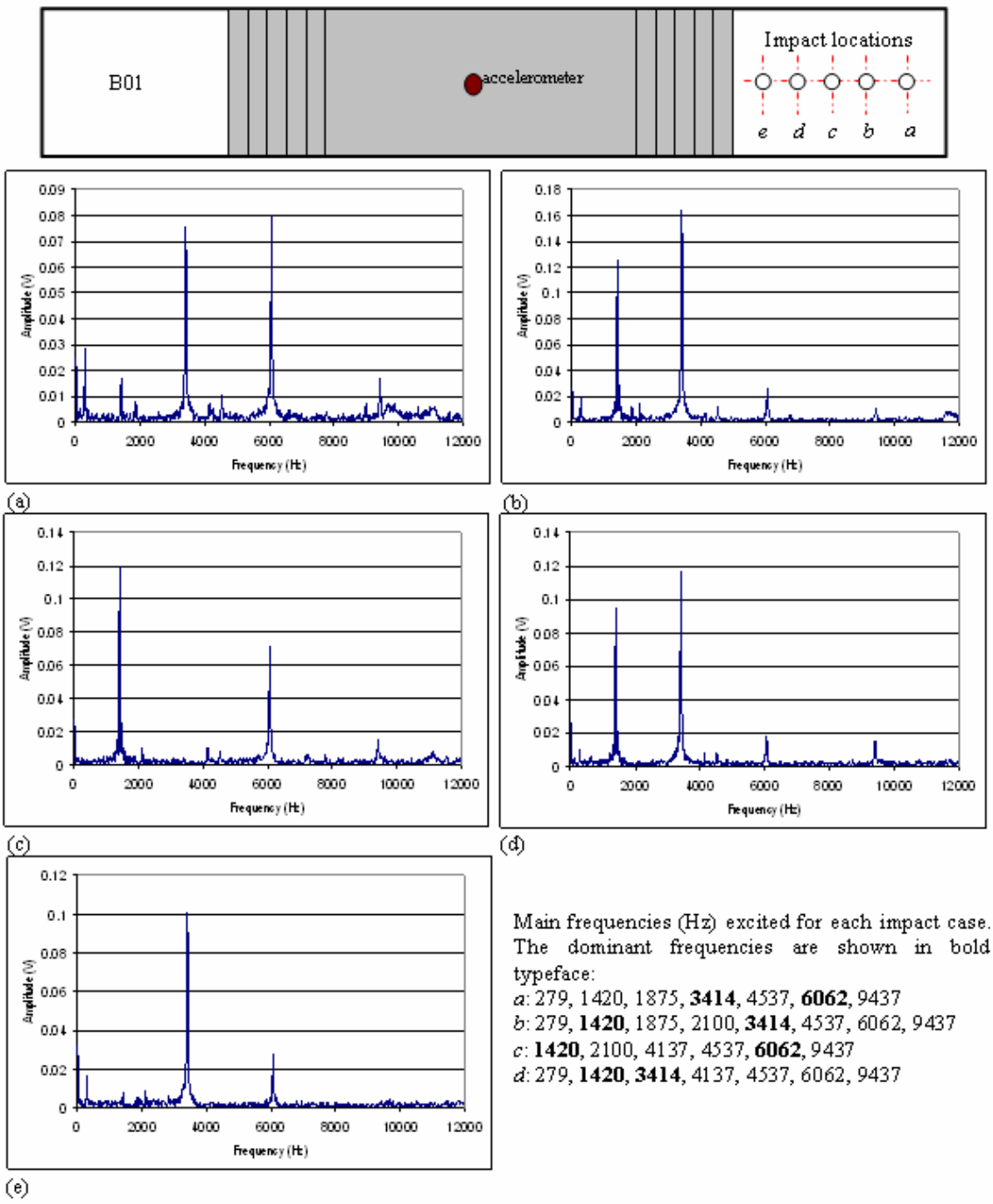

Figure 15: Top: Schematic of beam B01 with the locations of the accelerometer and five impact locations. (a) Frequency response obtained from impact location a. (b) Frequency response obtained from impact location b. (c) Frequency response obtained from impact location c. (d) Frequency response obtained from impact location d. (e) Frequency response obtained from impact location e.

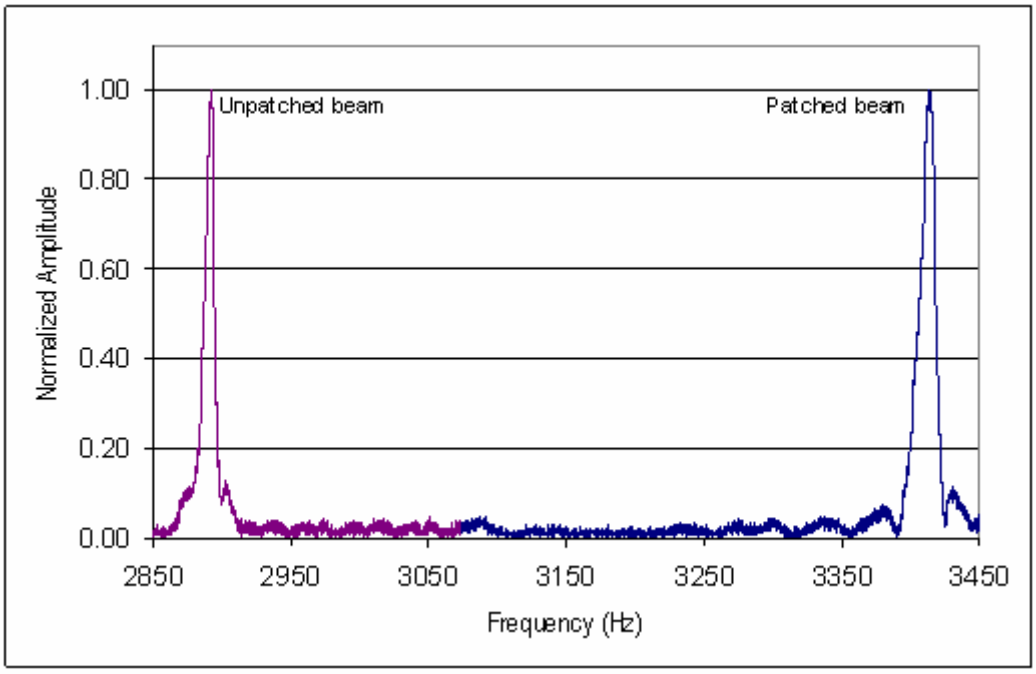

Figure 16: Frequency responses obtained for the B00 unpatched beam and B01 patched beam.

Similarly, for patched specimens with various respective disbond (B03, B05, B07), the shift in the natural frequency due to the relative reduction in the stiffness of the beam may also be tracked and the disbond can be quantified as illustrated in Table 2, where the theoretical values for the unpatched specimen (B00) were calculated using Equation (1) [33].

$$f_i = \frac{\lambda_i}{2\pi}\sqrt{\frac{Eh^2}{12\rho L^4}} \tag{1}$$

In Equation (1) f_i represents the frequency, λ_i the modal eigenvalue, E Young's modulus (68.9 GPa), h the thickness of the beam, ρ the density (2700kg/m^3), and L the length of the beam.

Table 2: A comparison of the natural frequencies obtained as a function of the patch and patch disbond. Theoretical values are shown for the unpatched specimen.

Frequency band	Unpatched specimen		Patched specimens			
	Exp. (Hz)	Theo. (Hz)	B01 Exp. (Hz)	B03 Exp. (Hz)	B05 Exp. (Hz)	B07 Exp. (Hz)
1	218	216	279	278	274	270
2	1172	1169	1420	1419	1399	1383
3	2892	2890	3414	3410	3369	3343

The higher frequencies are more sensitive to disbond progression due to wider band width available over the full disbond range. This is shown in Figure 18. Hence, the selection of a higher frequency will lead to a better degree of accuracy when characterizing the disbond based on the frequency response of the structure.

The variation in the frequencies obtained in Figure 17 for the three frequency bands indicate that the disbond influences the stiffness of the beam. Therefore, despite the increase in mass of the beams due to the bonded patch, the overall effect is a strengthening or stiffening of the beams. In this regard, the ability to predict the relative amount of disbond based on a reduction in stiffness would be an invaluable tool for SHM. Therefore by generating calibration curves for the 3 frequency bands it would be possible to estimate any amount of disbond *a priori* based on the frequency response obtained for a given patched beam.

Shown in Figure 19 are the calibration curves for the three frequency bands presented herein. The fitted curve is based on a 2^{nd} order polynomial. The equation of the polynomials is also shown for each case. It is interesting to note that for each of the frequency bands presented in Figure 19, the experimental result for beam specimen B03 does not fall on the fitted curve. This would suggest that the disbond is actually less than that. Hence, these curves can be used to predict the amount of disbond present in a patched beam by measuring the natural frequency obtained through impact hammer or coin tap excitation. Given in Table 3 are the polynomial equations defining the frequency dependence as a function of the amount of disbond for each of the three bands investigated.

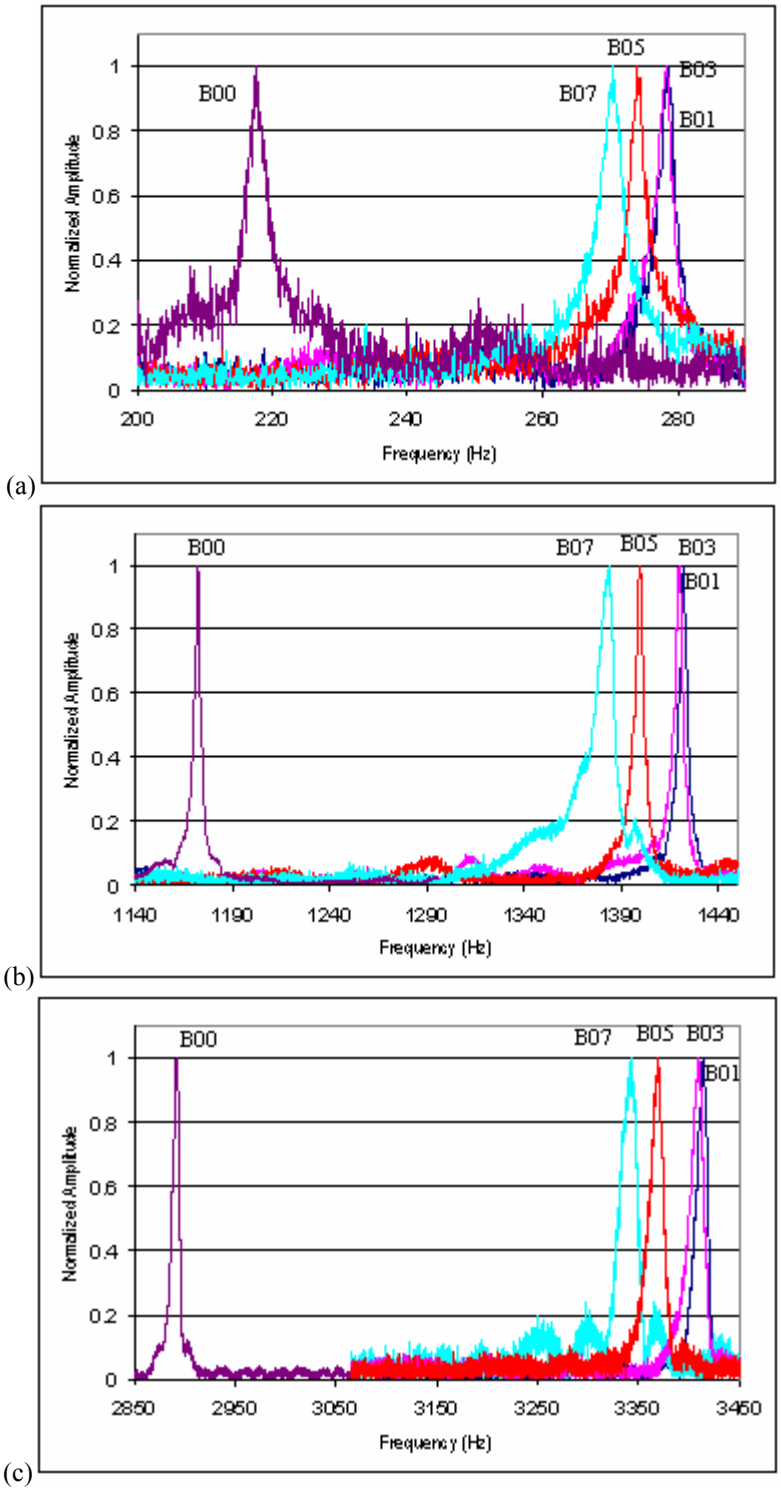

Figure 17: Comparisons of the shift in natural frequency due to the bonded patch and the shift due to relative disbond present in each specimen. (a) Frequency band 1. (b) Frequency band 2. (c) Frequency band 3.

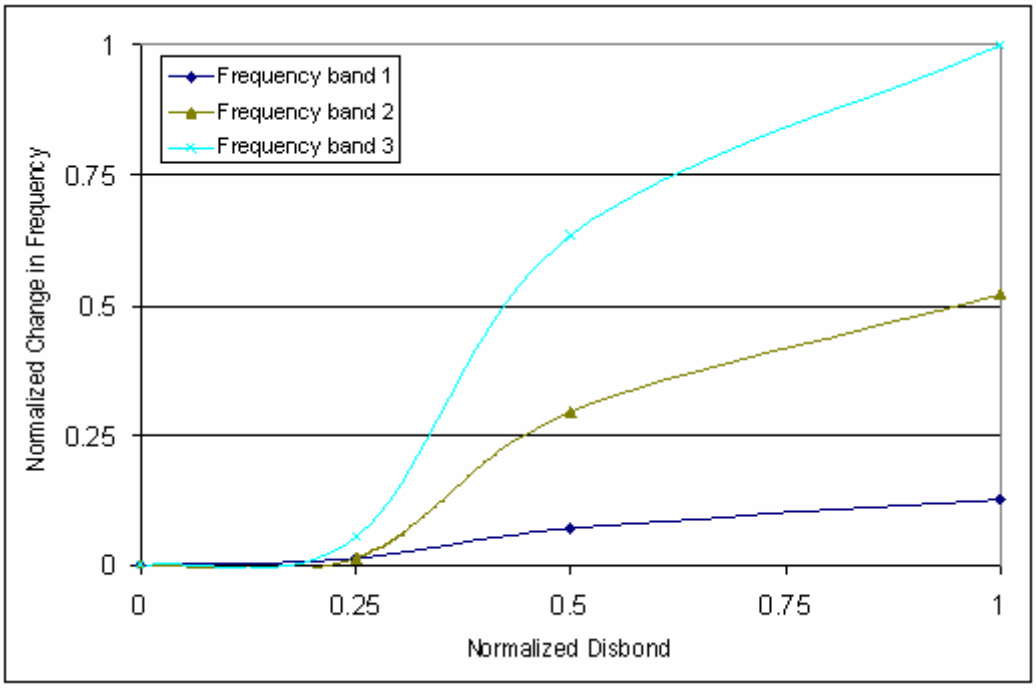

Figure 18: A comparison of the normalized change in frequency for each frequency band with respect to the amount of normalized disbond present in the structure.

Table 3: 2nd order polynomial equation for each of the frequency bands.

Frequency band	Polynomial equation
1	$2x^2 - 11x + 279$
2	$10x^2 - 47x + 1420$
3	$38x^2 - 109x + 3414$

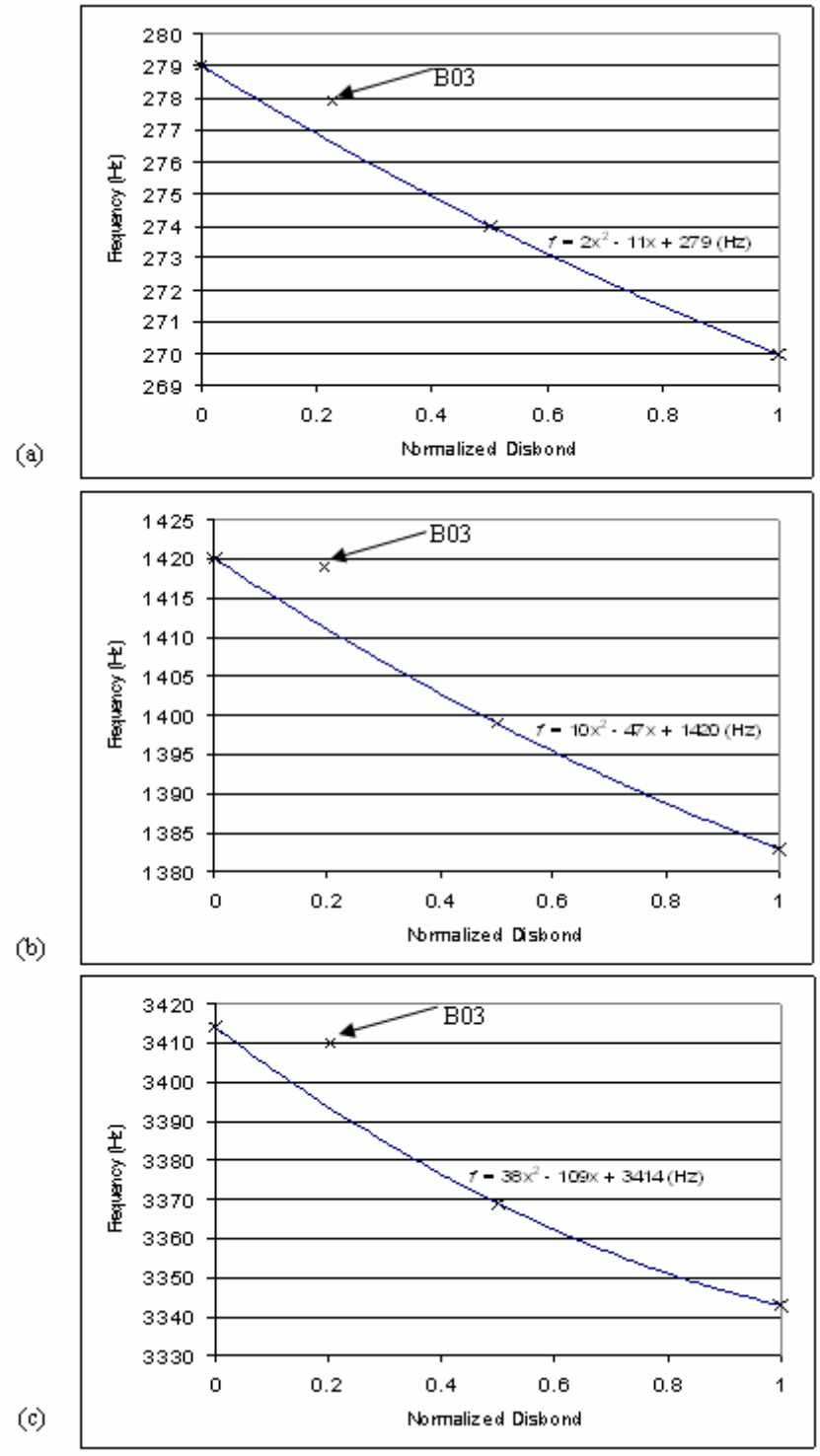

Figure 19: Calibration curves for the three frequency bands investigated (patched specimens only). (a) Frequency band 1. (b) Frequency band 2. (c) Frequency band 3. The experimental result for the B03 beam does not fall on the curve.

3.4 Thermal influences

Thermal effects will affect the mechanical properties of Al [34-36]. In terms of frequency based measurements, temperature will affect Young's modulus of elasticity and the density of Al. Therefore in order to quantify the change in frequency due to a disbond the temperature component should also be investigated. For the unpatched B00 beam, the temperature dependence of the natural frequency can be estimated by modifying Equation (1) to,

$$f_i(T) = \frac{\lambda_i}{2\pi}\sqrt{\frac{E(T)h^2(T)}{12\rho(T)L^4(T)}} \tag{2}$$

where the following definitions apply,

$$L(T) = L + \Delta L; \quad \Delta L = L * CTE * \Delta T \tag{2a}$$

$$h(T) = h + \Delta h; \quad \Delta h = h * CTE * \Delta T \tag{2b}$$

$$w(T) = w + \Delta w; \quad \Delta w = w * CTE * \Delta T \tag{2c}$$

where CTE is the coefficient of thermal expansion for 6061-T651 aluminum and *w* is the width of the beam.

$$\rho(T) = \frac{\rho L w h}{L(T)w(T)h(T)} \tag{2d}$$

$$E(T) = E + \Delta E; \quad \Delta E = E * CY * \Delta T \tag{2e}$$

$$\Delta T = T - T(21^{\circ}C) \tag{2f}$$

The thermal dependence of Al 6061-T651 on its mechanical characteristics is linear in nature [37], hence the linear changes in geometry due to the thermal influence can be readily calculated. In this regard, the CTE value for Al 6061-T651 employed in the theoretical calculations is 23.6μm/m-^{o}C [36-39], and the thermal dependence of the CTE in the temperature range -25^{o}C to 21^{o}C is 0.037142857140μm/m-^{o}C [39]. At temperatures between 21^{o}C-100^{o}C the CTE remains constant [38]. In the experiments carried herein, the temperature ranged between 22^{o}C to 70oC. For the thermal dependence of Young's modulus, the coefficient (CY) value of -0.042985714 GPa was determined experimentally and is consistent with the published value of -0.045 GPa [37]. The experimentally determined value was used for the theoretical analysis. In these tests, the beams were allowed to "soak" in a thermal environment for 90 minutes. Shown in Figure 20 is the B03 beam mounted in the oven (VWR Scientific Instruments Oven Model 1680). The surface temperature of the beam was measured and monitored using a thermometer (Omega Model HH21 Microprocessor Thermometer) and thermo-couple (Omega Type K) that was attached with an adhesive strip to the surface of the beam.

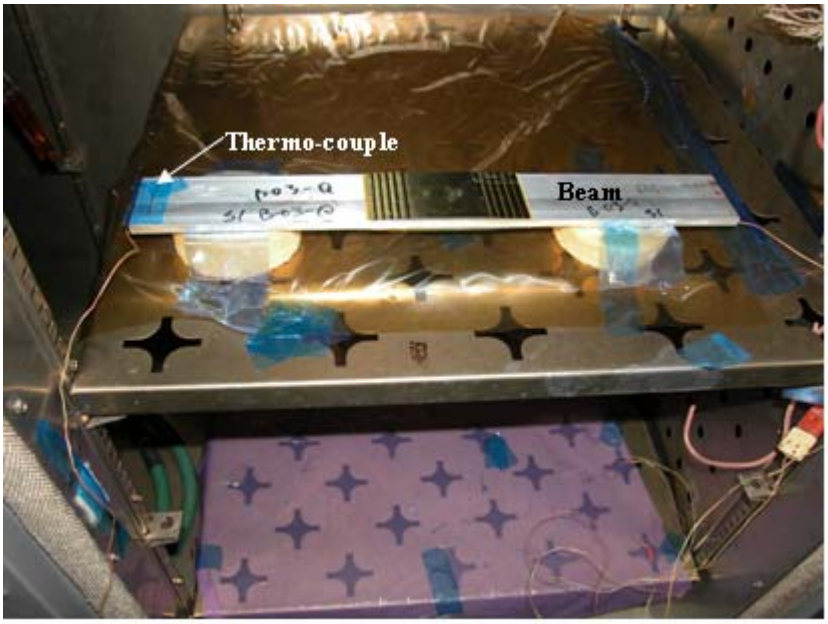

Figure 20: Placement of the beam in the thermal environment (oven). B03 beam is shown with the thermo-couple attached.

Due to the limitations in affixing the accelerometer at the *Top* position when the beam was thermally loaded, a different approach was employed to extract the frequency response of the beam. For these tests a micro-electro-mechanical-systems (MEMS) microphone was employed to acquire the acoustic signal from the surface of the beam after an applied tap. Shown in Figure 21 is an overview of the microphone assembly. Illustrated in Figure 22 is the beam mounted on the supports and placed over the microphone. Shown in Figure 23 is an overview of the entire experimental setup.

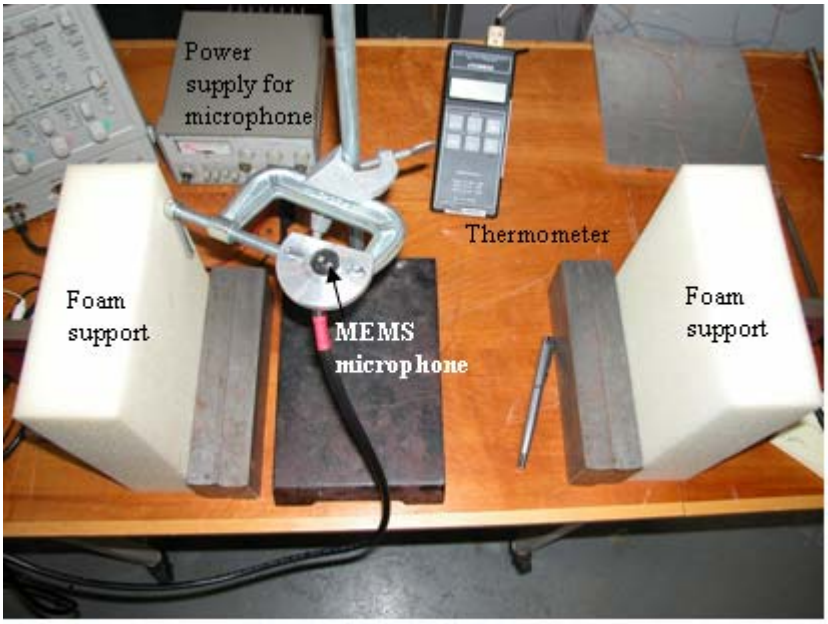

Figure 21: An overview of the experimental setup used for the temperature measurements.

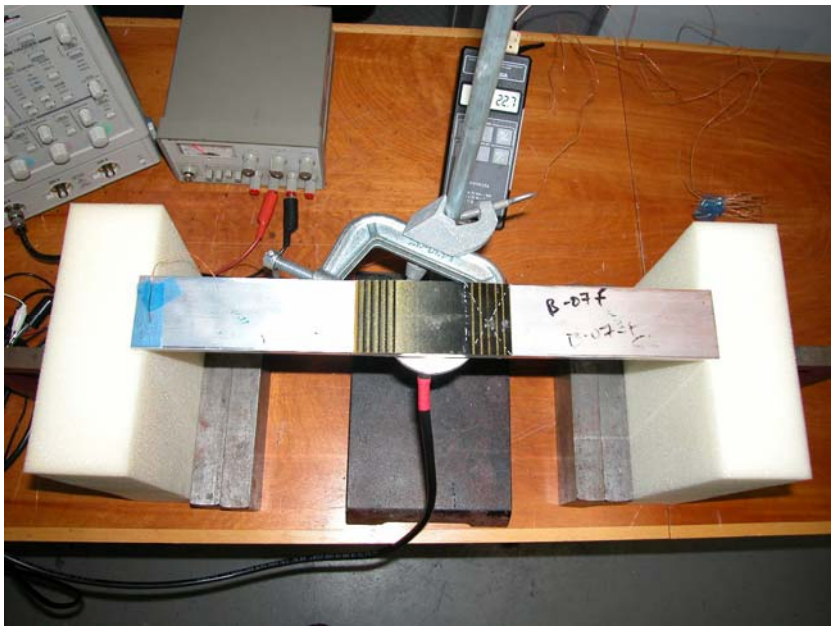

Figure 22: The aluminum beam placed over the microphone.

Figure 23: An overview of the experimental setup employed for the temperature tests.

Tap tests were then taken for every 5 or 10 degree centigrade decrease in the surface temperature of the beam. Shown in Figure 24 are the superimposed frequency responses obtained at various temperatures for the unpatched B00 beam. It can clearly be seen that the frequency response obtained is a function of the surrounding temperature. Figure 25a shows the experimental results for the shift in frequency of the B00 beam and the linear fit, Figure 25b shows the experimental results for both the B01 and B07 specimens as function of temperature and the respective 2nd order polynomial fit. The non-linearity of the responses obtained for the patched B01 and B07 specimens are in part due to the thermal coefficient mismatches between the 6061-T651 Al and the bonded patch material and the thermal characteristics of the patch material. It can be seen in Figure 25b that at higher temperatures the stiffening effect due to the patch reduces non-linearly and that the non-linearity is increased further for a beam specimen with a disbond present. Given in Table 4 are the equations used to generate the curves to compare with the experimental results.

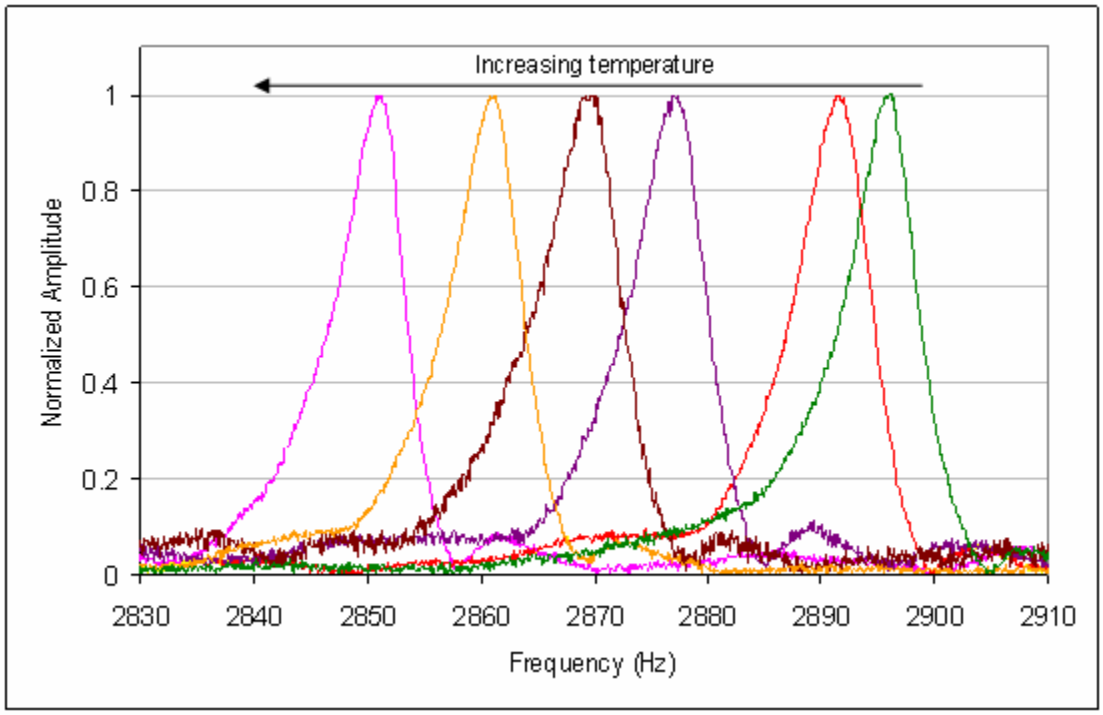

Figure 24: The variation of the frequency response as a function of the thermal environment for the B00 unpatched beam.

Table 4: The equations used to generate the fitted curves for the 3 beams investigated.

Beam	Equation
00	$-0.9246T + 2911.8$
01	$-0.0047T^2 - 0.4214T + 3423.4$
07	$-0.0092T^2 - 0.4524T + 3349.9$

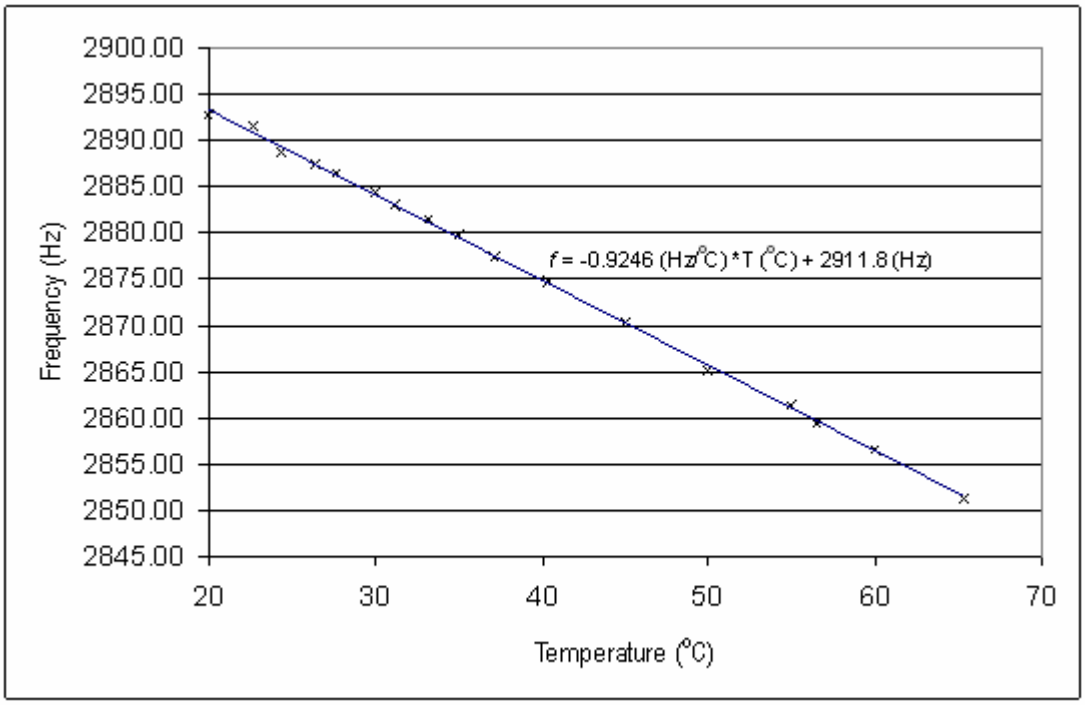

(a)

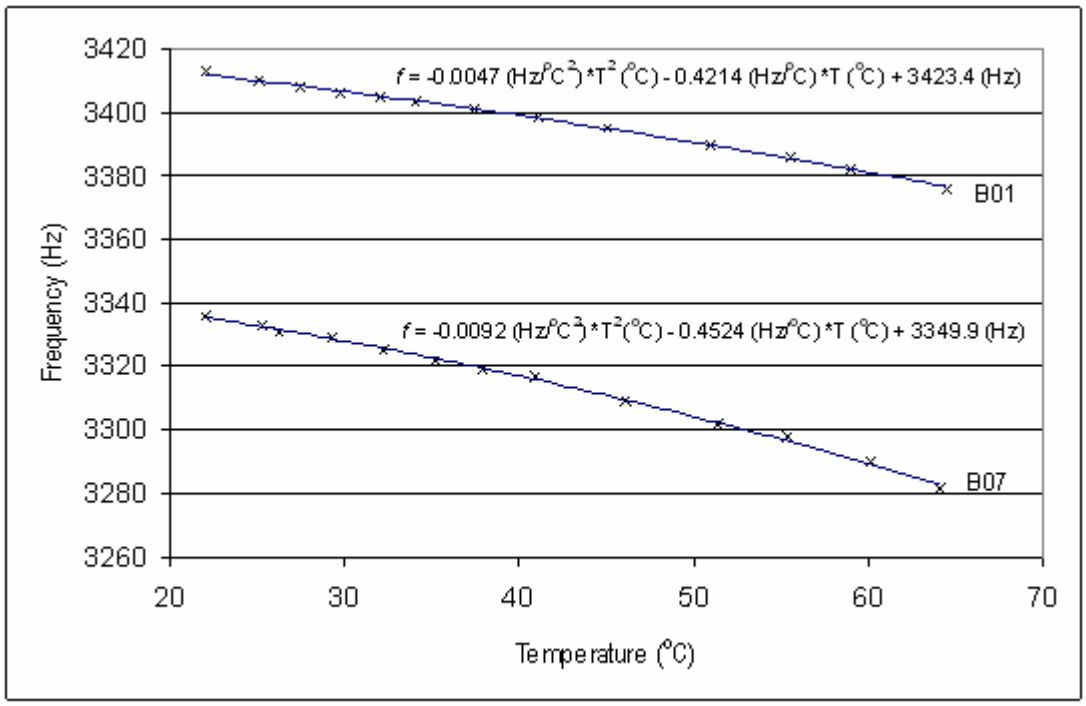

(b)

Figure 25: The influence of temperature on the natural frequency response. (a) The linear response of the B00 beam. (b) Comparing the non-linear responses of the B01 and B07 beams.

4. Conclusions

A simple, practical, potentially deployable method has been demonstrated to characterize the disbond of bonded patch repair. The ease of this approach allows one to employ the classical coin tap method to excite the beam. The shift in natural resonance frequency was employed to obtain information about the status of the bonded patch. Three frequency ranges were investigated. It was determined that higher frequencies showed better resolution when measuring the amount of disbond. The effect of modal impact location and temperature were also presented in order to demonstrate their influence on the frequency spectrum obtained.

The proposed approach presents a real potential for integration into a maintenance program due to its analysis and implementation simplicity as well as system portability. Moreover it is quick and inexpensive, which can reduce maintenance cost associated with inspection and maintenance of bonded repairs.

The work presented herein was demonstrated on a simple specimen that has Teflon film to simulate patch disbonds. Future work should be carried out to demonstrate the same approach on natural disbonds within a specimen that is more representative of actual aircraft structure. In this case, patch disbond integrity, severity and progression could be determined while a patch repair is undergoing fatigue cycle. The possibilities of demonstrating this technique on a real aircraft structure should also be looked at.

References

[1] Roach, D., "Further Evolution of Composite Doubler Aircraft Repairs Through a Focus on Niche Applications", FAA Airworthiness Assurance Center, Sandia National Laboratories.

[2] Roach, D. and Rackow, K., "Health Monitoring of Aircraft Structures Using Distributed Sensor Systems", FAA Airworthiness Assurance Center, Sandia National Laboratories.

[3] Black, S. Technical Editor (2008), "Structural Health Monitoring: Composites Get Smart", *Composites World-High Performance Composites*, Gardner Publications.

[4] http://www.airforce.forces.gc.ca/v2/netpub/index-eng.asp?mode=1.

[5] Hafesjee, J. Managing Editor (2007), "Self-Powered Health-Reporting Patch for Aircraft", Australian Defence Science, vol. 15.

[6] Clark, R. J. and Romilly, D. P. (2007), "Bending of Bonded Composite Repairs for Aluminum Aircraft Structures: A Design Study", *Journal of Aircraft*, vol. 44, pp.2012-2025.

[7] Galea, S., McKenzie, I., Chester, R., Lloyd, P., Jogia, M. and Mrad, N. (2000), "Embedded Sensors in Repair Patches", TTCP Technical Report, Operating Assignment 0-9, TR-MAT-TP7-2-2000.

[8] Koh, Y. L., Chiu, W. K., Marshall, I. H., Rajic, N. and Galea, S. C. (2001), "Detection of Disbonding in a Repair Patch by Means of an Array of Lead Zirconate Titanate and Polyvinylidene Fluoride Sensors and Actuators", *Smart Materials and Structures*, vol. 10, pp. 946-962.

[9] Pan, X. W., Liang, D. and Li, D. (2006), "Optical Fiber Sensor Layer Embedded in Smart Composite Material and Structure", *Smart Materials and Structures*, vol. 15, pp. 1231-1234.

[10] Albat, A. (1997), "Investigation of Failure Initiation Models for Bonded Composite Patches on Metallic Structures-Residual Strain Measurements", Final Report 31184-6-0161/001/ST.

[11] Dasgupta, A. and Pecht, M. (1991), "Material Failure Mechanisms and Damage Models", *IEEE Transactions on Reliability*, vol. 40, pp. 531-536.

[12] Olson, S. P., Castracane, J. and Spoor, R. E. (2008), "Piezoresistive Strain Gauges for use in Wireless Component Monitoring Systems", IEEE Symposium on Sensor Applications, Atlanta, GA, USA, February 12-14.

[13] Gorinevsky, D., Gordon, G. A., Beard, S., Kumar, A. and Chang, F.-K. (2005), "Design of Integrated SHM System for Commercial Aircraft Applications", 5th International Workshop on Structural Health Monitoring, Stanford, CA, USA.

[14] Chaudhry, Z., Joseph, T., Sun, F. and Rogers, C. (1995), "Local-Area Health Monitoring of Aircraft via Piezoelectric Actuator/Sensor Patches", *Proceedings of SPIE*, vol. 2443, pp. 268-276.

[15] Galea, S. C., Chiu, W. K. and Paul, J. J. (1993), "Use of Piezoelectric Films in Detecting and Monitoring Damage in Composites", *Journal of Intelligent Material Systems and Structures*, vol. 4, pp. 330-336.

[16] Whittingham, B., Li, H. C. H., Herszberg, I. and Chiu, W. K. (2006), Disbond Detection in Adhesively Bonded Composite Structures using Vibration Signatures", *Composite Structures*, vol. 75, pp. 351-363.

[17] Wu, H. and Siegel, M. (2000), "Correlation of Accelerometer and Microphone Data in the "Coin Tap Test", *IEEE Transactions on Instrumentation and Measurement*, vol. 49, pp. 493-497.

[18] Meirovitch, L. (1980), Computational Methods in Structural Dynamics, Sijthoff and Noordhoff Publishers, ISBN 90-286-0580-0.

[19] White, C., Whittingham, B., Li, H. C. H., Herszberg, I. and Mouritz, A. P. (2007), "Vibration Based Structural Health Monitoring of Adhesively Bonded Composite Scarf Repairs", 5th Australasian Congress on Applied Mechanics, Brisbane, Australia, 10-12 December.

[20] Cawley, P. and Adams, R. D. (1988), "The Mechanics of the Coin-Tap Method of Nondestructive Testing", *Journal of Sound and Vibration*, vol. 122, pp. 299-316.

[21] Zou, Y., Tong, L. and Steven, G. P. (2000), "Vibration-Based Model-Dependent Damage (Delamination) Identification and Health Monitoring for Composite Structures-A Review", *Journal of Sound and Vibration*, vol. 230, pp. 357-378.

[22] Soutis, C. and Hu, F. Z. (1997), "Design and Performance of Bonded Patch Repairs of Composite Structures", *Proceedings of the Institution of Mechanical Engineers: Part G*, vol. 11, pp. 263-271.

[23] Hahn, G. (2002), "Qualifying New Technology for Deepwater Oil and Gas Development", Minerals Management Service-Offshore Technology Research Center (MMS-OTRC) Workshop, Houston, Texas, USA, 29-30 October.

[24] Chen, J.-Y., Hoa, S. V., Jen, C.-K., Viens, M. and Monchalin, J.-P. (1998), "Ultrasonic Evaluation of Graphite/Epoxy Composites with Different Curing Conditions", *Polymer Composites*, vol. 19, pp. 225-232.

[25] Ninan, L., Tsai, J. and Sun, C. T., (2001), "Use of Split Hopkinson Pressure Bar for Testing Off-Axis Composites", *International Journal of Impact Engineering*, vol. 25, pp. 291-313.

[26] Bing, Q. and Sun, C.T. (2005), "Modeling and Testing Strain Rate-Dependent Compressive Strength of Carbon/Epoxy Composites", *Composites Science and Technology*, vol. 65, pp. 2481-2491.

[27] Shivakumar, K. N., Allen, H. G. and Avva, V. S. (1994), "Interlaminar Tension Strength of Graphite/Epoxy Composite Laminates", *AIAA Journal*, vol. 32, pp. 1478-1484.

[28] Hexcel, Product Data Sheet (2009): AS4/3501-6 Carbon/Epoxy Unidirectional Prepreg, www.hexcel.com.

[29] Hale, R. D., Associate Professor Aerospace Engineering, The University of Kansas, 2004 Learned Hall, Lawrence, KS, USA 66045-2221.

[30] Department of Chemistry, University of Wisconsin-Madison, 1101 University Avenue, Madison, Wisconsin, USA, 53706-1396, www.chem.wisc.edu.

[31] Cho, J., Chen, J. Y. and Daniel, I. M. (2007), "Mechanical Enhancement of Carbon Fiber/Epoxy Composites by Graphite Nanoplatelet Reinforcement", *Scripta Materialia*, vol. 56, pp. 685-688.

[32] Cytex, Technical Data Sheet (2009): FM®73 Toughened Epoxy Film, www.cytec.com.

[33] Harris, C. M. and Crede, C. E. (1976), Shock and Vibration Handbook, McGraw-Hill Book Company, ISBN 0-07-026799-5, page 1-14.

[34] Davidson, P. and Davis, R. (1975), "Mechanical Behavior of 6061-T651 Aluminum", *AIAA Journal*, vol.13, pp.1547-1548.

[35] Martin, W. R. and Weir, J. R. (1964), "Mechanical Properties of X8001 and 6061 Aluminum Alloys and Aluminum-Base fuel Dispersion at Elevated Temperatures", ORNL, Oak Ridge, Tennessee, USA.

[36] Augereau, F., Laux, D., Allais, L., Mottot, M. and Caes, C. (2007), "Ultrasonic Measurement of Anisotropy and Temperature Dependence of Elastic Parameters by a Dry Coupling Method Applied to a 6061-T6 Alloy", *Ultrasonics*, vol. 46, pp. 34-41.

[37] Aerospace Specification Metals Inc. (ASM) (2009), Material Data Sheet: Aluminum 6061-T6; 6061-T651.

[38] Owolabi, G. M., Odeshi, A. G., Singh, M. N. K. and Bassim, M. N. (2007), "Dynamic Shear Band Formation in Aluminum 6061-T6 and Aluminum 6061-T6/Al_2O_3 Composites", *Materials Science and Engineering*, vol. 457, pp. 114-119.

[39] Kang, S.-G., Kim, M.-G. and Kim, C.-G. (2007), "Evaluation of Cryogenic Performance of Adhesives using Composite-Aluminum Double-Lap Joints", *Composite Structures*, vol. 78. pp. 440-446.This is fictional text to check hanging indent of a reference paragraph. This is fictional text to check hanging indent of a reference paragraph.

List of symbols/abbreviations/acronyms/initialisms

a	base excitation impact location designation
Al	aluminum
b	base excitation impact location designation
Beam	accelerometer placement designation
Bottom	accelerometer placement designation
B00	bare aluminum beam
B01	patched aluminum beam no-disbond
B03	patched aluminum beam -disbond
B05	patched aluminum beam -disbond
B07	patched aluminum beam full-disbond
c	base excitation impact location designation
CF	Canadian Forces
CTE	coefficient of thermal expansion
CY	coefficient of thermal dependence for Young's modulus
°C	degrees centigrade
d	base excitation impact location designation
e	base excitation impact location designation
E	Young's modulus of elasticity
Exp.	experimental (results)
f	frequency
GPa	giga Pascal (1 billion Pascal)
Gr/Ep	graphite/epoxy
h	thickness
Hz	hertz
kg	kilogram (1 thousand grams)
L	length
m	meter
min	minute
mm	millimeter (1 thousandth of a meter)
MEMS	micro-electro-mechanical-systems
MPa	mega Pascal (1 million Pascal)

NDI	non-destructive inspection
P	pressure
Psig	pounds-per-square-inch gauge
s	second (time)
SHM	structural health monitoring
T	temperature
(T)	indicates temperature dependent variable
Theo.	theoretical (results)
Top	accelerometer placement designation
V	volt
w	width
x	normalized disbond variable (varies between 0 and 1)
λ	modal eigenvalue
μ	micro (1 millionth)
π	pi
ρ	density
1	frequency band 200-290 Hz
2	frequency band 1140-1440 Hz
3	frequency band 2850-3450 Hz
(21^{o}C)	reference temperature
2^{nd}	second (numerical)
@	at
$	dollar
%	percent

Distribution list

Document No.: DRDC Atlantic TM 2009-079

LIST PART 1: Internal Distribution by Centre:

1 DG / DRDC Atlantic
1 H / AVRS
7 AVRS
5 DRDC Atlantic Library

14 TOTAL LIST PART 1

LIST PART 2: External Distribution by DRDKIM

National Defence Headquarters
101 Colonel By Drive
Ottawa, ON
K1A 0K2

1 DRDKIM
1 Assoc, DGRPD
1 DSTA
1 DTAES
1 DTAES 7
4 DTAES 7-7
1 Library & Archives Canada, Attn: Military Archivist, Government Records Branch

10 TOTAL LIST PART 2

24 TOTAL COPIES REQUIRED

This page intentionally left blank.

DOCUMENT CONTROL DATA

(Security classification of title, body of abstract and indexing annotation must be entered when the overall document is classified)

1. ORIGINATOR (the name and address of the organization preparing the document. Organizations for whom the document was prepared, e.g. Centre sponsoring a contractor's report, or tasking agency, are entered in section 8.)

DRDC Atlantic / AVRS
9 Grove Street
Dartmouth, NS, B2Y 3Z7 Canada

2. SECURITY CLASSIFICATION (overall security classification of the document including special warning terms if applicable).

UNCLASSIFIED

3. TITLE (the complete document title as indicated on the title page. Its classification should be indicated by the appropriate abbreviation (S,C,R or U) in parentheses after the title).

Bonded-Patch Integrity Characterization: A Modal Resonance Approach

4. AUTHORS (Last name, first name, middle initial. If military, show rank, e.g. Doe, Maj. John E.)

Rinaldi, Gino; Genest, Marc

5. DATE OF PUBLICATION (month and year of publication of document)

September 2009

6a. NO. OF PAGES (total containing information Include Annexes, Appendices, etc).

50

6b. NO. OF REFS (total cited in document)

39

7. DESCRIPTIVE NOTES (the category of the document, e.g. technical report, technical note or memorandum. If appropriate, enter the type of report, e.g. interim, progress, summary, annual or final. Give the inclusive dates when a specific reporting period is covered).

Technical Memorandum

8. SPONSORING ACTIVITY (the name of the department project office or laboratory sponsoring the research and development. Include address).

Defence R&D Canada – Atlantic
PO Box 1012
Dartmouth, NS, Canada B2Y 3Z7

9a. PROJECT OR GRANT NO. (if appropriate, the applicable research and development project or grant number under which the document was written. Please specify whether project or grant).

9b. CONTRACT NO. (if appropriate, the applicable number under which the document was written).

10a ORIGINATOR'S DOCUMENT NUMBER (the official document number by which the document is identified by the originating activity. This number must be unique to this document.)

DRDC Atlantic TM 2009-079

10b OTHER DOCUMENT NOs. (Any other numbers which may be assigned this document either by the originator or by the sponsor.)

11. DOCUMENT AVAILABILITY (any limitations on further dissemination of the document, other than those imposed by security classification)

(x) Unlimited distribution
( ) Defence departments and defence contractors; further distribution only as approved
( ) Defence departments and Canadian defence contractors; further distribution only as approved
( ) Government departments and agencies; further distribution only as approved
( ) Defence departments; further distribution only as approved
( ) Other (please specify):

12. DOCUMENT ANNOUNCEMENT (any limitation to the bibliographic announcement of this document. This will normally correspond to the Document Availability (11). However, where further distribution (beyond the audience specified in (11) is possible, a wider announcement audience may be selected).

13. ABSTRACT (a brief and factual summary of the document. It may also appear elsewhere in the body of the document itself. It is highly desirable that the abstract of classified documents be unclassified. Each paragraph of the abstract shall begin with an indication of the security classification of the information in the paragraph (unless the document itself is unclassified) represented as (S), (C), (R), or (U). It is not necessary to include here abstracts in both official languages unless the text is bilingual).

Bonded-patch technology can be employed to either enhance the integrity or to repair damaged structures. In aerospace applications consideration must be given to the effectiveness of the bonded-patch technology to restore the performance of a given component to an acceptable level. Repair of aircraft and components is of particular importance for military air fleets due to the prolonged life-cycle of the aircraft beyond the normal design life. In this respect, a reliable and cost-effective repair technology would help to minimize costs associated with maintenance of military air fleets by offering a low cost alternative to replacing aircraft components. A fundamental drawback to the application of this technology, particularly for critical, primary structure, is the need to assure that the patch is performing as designed. Hence, the on-component characterization of a given bonded-patch is of vital importance in terms of assessing the integrity of the bond. Disbond or delamination associated with long-term stress cycling can adversely affect the quality of the bonded-patch. In this report, a simple and reliable method based on modal resonance is described in which the variation in the modal resonance is employed to detect and monitor the evolution of a bonded-patch disbond. For demonstration purposes the proposed method is applied to aluminum 6061-T651 beams with bonded-patch segments on their surface.

14. KEYWORDS, DESCRIPTORS or IDENTIFIERS (technically meaningful terms or short phrases that characterize a document and could be helpful in cataloguing the document. They should be selected so that no security classification is required. Identifiers, such as equipment model designation, trade name, military project code name, geographic location may also be included. If possible keywords should be selected from a published thesaurus. e.g. Thesaurus of Engineering and Scientific Terms (TEST) and that thesaurus-identified. If it not possible to select indexing terms which are Unclassified, the classification of each should be indicated as with the title).

Bonded-patch technology, Structural enhancement, Structural health monitoring, Modal resonance, Vibration analysis, Aluminum 6061-T651

This page intentionally left blank.

Defence R&D Canada

Canada's leader in defence
and National Security
Science and Technology

R & D pour la défense Canada

Chef de file au Canada en matière
de science et de technologie pour
la défense et la sécurité nationale

www.drdc-rddc.gc.ca